JOURNAL OF Materials CHEMISTRY

Sol–gel synthesis of alumina modified by phosphorus: a solid state NMR characterization study

Juliette Quartararo,[a] Michel Guelton,[a] Monique Rigole,[a] Jean-Paul Amoureux,[b] Christian Fernandez[c] and Jean Grimblot*[a]

[a]*Laboratoire de catalyse, UPRESA 8010, Université des Sciences et Technologies de Lille, Bâtiment C3, 59655 Villeneuve d'Ascq Cédex, France. email: jean.grimblot@univ-lille1.fr*
[b]*Laboratoire de dynamique et structure des matériaux moléculaires, URA CNRS 801, Université des Sciences et Technologies de Lille, Bâtiment P5, 59655 Villeneuve d'Ascq Cédex, France*
[c]*Laboratoire de catalyse et spectrochimie, UMR 6506, ISMRA, Université de Caen, 6 boulevard du Maréchal Juin, 14050 Caen Cédex, France*

Received 17th May 1999, Accepted 14th July 1999

A sol–gel method using aluminium tri(*sec*-butoxide) and orthophosphoric acid, H_3PO_4, as the Al and P sources respectively, 2-butanol as the solvent and 1,3-butanediol as the chelating agent has been extensively used to prepare P-alumina catalytic supports. The study was particularly focused on the influence of the step of phosphorus introduction during the sol–gel procedure, on the amount of incorporated phosphorus and on the temperatures of drying and calcination of the gels to obtain the final mixed oxides. In addition to the classical chemical composition determinations and measurements of specific surface area, characterisations were mainly performed by using solid state ^{27}Al and ^{31}P MAS NMR. More precise determinations of the nature of aluminium sites were also obtained by ^{27}Al MQMAS NMR. XRD was also used to a lesser extent.

Poorly crystallised boehmite is present in the dried samples with aluminium mainly localised in octahedral sites whereas phosphorus is detected as monomeric and polymeric phosphates whose proportions depend on the phosphorus content. For the highest P/Al ratio (P/Al = 0.2) and when phosphorus is introduced with the hydrolysis water, the NMR data reveal the presence of bridged entities such as Al_{tetra}–O–P.

After calcination at 500 °C, badly crystallised γ-alumina is formed with octahedral, pentacoordinate and tetrahedral aluminium sites. For the highest phosphorus loading, a new aluminium site corresponding to the presence of $AlPO_4$ is observed. The values of the second order quadrupolar effect for each species depend on the preparation procedure and characterise the degree of distortion of the aluminium sites.

The drying temperature up to 200 °C does not modify the gel structure whereas transformation of boehmite into alumina occurs above 350 °C and, for the highest phosphorus content, there is partial destruction of alumina to form aluminium phosphate when the temperature of calcination is increased. Such an increase also has a non-negligible influence on the specific surface area which, however, remains as high as 350 $m^2 g^{-1}$ after calcination at 700 °C.

Introduction

Hydrotreating catalysis is aimed at the removal, under hydrogen pressure, of heteroatoms like sulfur, nitrogen or some metals (V, Ni) molecularly bound to hydrocarbons constituting petroleum fractions. The hydroprocessing reactions (hydrodesulfurization HDS, hydrodenitrogenation HDN, and hydrodemetallation HDM) deserve considerable interest in the petroleum industry, namely because they permit the production of chemicals, gasoline, gas-oil or fuels of high quality as required by environmental legislation. The active phase of hydrotreating catalysts is generally composed of nanocrystallites of MoS_2 or WS_2 promoted by an element such as cobalt or nickel.[1,2] γ-Alumina is the preferred support as it permits the optimization of the dispersion of the active phase on its surface. However, activity increases in HDS, HDN or HDM reactions can be induced by chemical modifications of the support. In particular, the introduction of rather small amounts of phosphorus (up to *ca.* 10 wt% of P) in/on alumina may induce interesting changes in terms of catalytic behavior.[3,4] However, the influence of phosphorus in hydrotreating catalysis is not always clearly understood.[5] It may increase the activity but it may also have a negative influence, depending on its total amount and on the considered reaction. It has been claimed that the presence of phosphorus modifies the texture and acidity of the catalysts or induces the creation of new active sites. Moreover, Jian and Prins[6] found that the effect of phosphorus depends on the nature of the reactants and intermediates. For example, indole or quinoline HDN is improved by phosphorus addition,[7–9] whereas negative effects have been observed for pyridine HDN.[6] Rigorous control of the preparation conditions is crucial to optimise the beneficial introduction of phosphorus into a hydrotreating catalyst. This is the major goal of the present study: what is the interaction between the phosphorus oxo species and the alumina framework, and where are the phosphorus atoms located? These questions will be addressed by examining P-alumina mixed oxides prepared by a sol–gel method. Indeed, the sol–gel preparation method has been shown to be well suited for the synthesis of hydrotreating catalysts.[10,11] It permits the amount of well dispersed molybdenum oxo species in the catalyst formulation to be increased, and enables the formation of solids with high specific surface area (about 500 $m^2 g^{-1}$). Recently, this method has been used in our laboratory to prepare molybdenum-based catalysts modified by phosphorus that was introduced as two precursors, H_3PO_4 and P_2O_5.[3] In the present study, we will restrict the study to the formation of P-Al_2O_3 supports with the use of H_3PO_4 as the phosphorus

source, as this allows the production of better catalysts.[3] X-Ray diffraction (XRD) is not the most convenient technique for the structural characterization of such solids, which are rather amorphous. In contrast, solid state nuclear magnetic resonance (NMR) is as a very interesting tool for the identification of the local environments of both P (^{31}P NMR) and Al (^{27}Al NMR). In particular, the combination of solid state ^{31}P and ^{27}Al magic-angle spinning NMR (MAS NMR) and two-dimensional ^{27}Al multiple-quantum magic-angle spinning NMR (MQMAS NMR) has shown promising results for Mo-P-alumina catalysts prepared by classical impregnation[12] or sol–gel methods.[13] The main conclusions we obtained indicate that most of the phosphorus is in close contact with the alumina, with the formation of aluminium phosphate in a monolayer structure.

In this work, we were mainly interested by (i) the influence of the step for the introduction of phosphorus during the sol–gel procedure leading to P-alumina mixed oxides, (ii) the amount of incorporated phosphorus, and (iii) the temperature of calcination of the dried gels. In addition to classical chemical composition determinations and textural characterizations, MAS and MQMAS NMR were used to observe the two elements (P and Al) in the oxide framework. XRD was also used to a lesser extent.

Experimental

Materials preparation

The preparation of the P-alumina mixed oxides (see Fig. 1) was conducted according to a sol–gel procedure described previously for the formation of pure alumina and alumina modified by Mo and/or P.[3,10,11,14] The alumina framework was obtained by hydrolysis of aluminium tri(*sec*-butoxide) [ASB, $Al(OC_4H_9)_3$] (from Fluka, purity $\geqslant$95%) dissolved first in its parent alcohol (2-butanol, from Fluka, purity $\geqslant$99.5%). 1,3-Butanediol (from Fluka, purity $\geqslant$98%), the chelating agent, was then added to the initial solution to provide better control over the hydrolysis step,[14] which was conducted with distilled water. After stirring the mixture for 1 h at 85 °C, followed by holding the gel in the solution at room temperature for 1 h, the solids were dried in two steps at 40 °C and then at 100 °C in the open air. At this stage, the solids are labelled with 'D'. The next step was calcination in flowing air in a quartz reactor, typically at 500 °C for 3 h, unless otherwise stated. The final oxides are labelled with 'C'. The phosphorus precursor (orthophosphoric acid, H_3PO_4, from Fluka, a solution containing 85% of phosphoric acid) was introduced at three different stages during the sample synthesis. The acid was introduced either with 2-butanol (samples P1), or with 1,3-butanediol (samples P2), or with water during the hydrolysis step (samples P3). In the sample nomenclature, the atomic ratio P/Al is indicated in parentheses. For example, sample P1(0.03)D-Al is a dried solid which has a P/Al ratio of 0.03 and for which the orthophosphoric acid was introduced with 2-butanol. The general procedure for the sol–gel mixed oxide preparation is reported in Fig. 1.

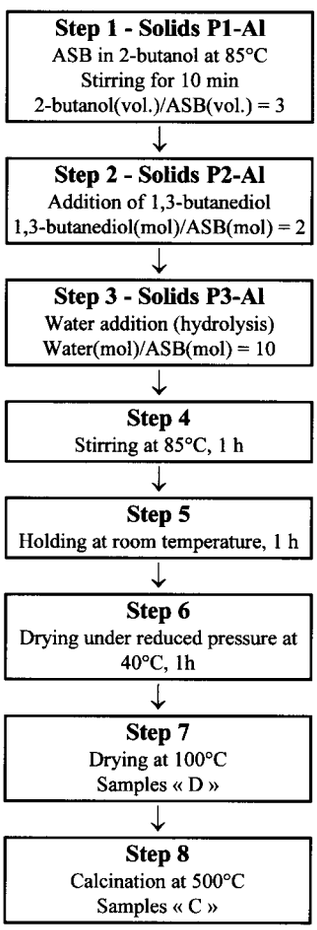

Fig. 1 Schematic description of the procedure for the preparation of P-alumina mixed oxides. Orthophosphoric acid is introduced at step 1 (samples P1), at step 2 (samples P2) or at step 3 (samples P3).

Solid characterization

The chemical compositions of the calcined mixed oxides were determined by the Service Central d'Analyses du CNRS (Vernaison, France). The specific surface areas of the calcined powders were calculated by the one-point BET isotherm adsorption of N_2 using a Quantasorb Jr sorptometer. The samples were pre-treated under flowing N_2 at 200 °C for 1 h prior to measurements. X-Ray diffraction patterns were obtained with a Siemens D5000 diffractometer equipped with a goniometer, a monochromator and a Cu X-ray tube.

Conventional ^{27}Al MAS NMR spectra were obtained with a Bruker ASX400 spectrometer. The resonance frequency was $\nu_0 = 104.26$ MHz, with a recycling time of 3 s and a short pulse time of 1 μs (flip angle $\approx \pi/12$). The spinning frequency was 15 kHz and $Al(H_2O)_6^{3+}$ was taken as a reference. ^{31}P MAS NMR spectra were obtained from a Bruker ASX100 spectrometer operating at a resonance frequency of $\nu_0 = 40.53$ MHz with a recycling time of 40 s and a pulse time of 2 μs (flip angle $\approx \pi/6$). The spinning frequency was 12.5 kHz and H_3PO_4 was taken as a reference.

The theoretical aspects of MQMAS (multiple-quantum magic-angle spinning) NMR can be found in references 15–18. The MQMAS measurements were performed with a three pulse *z*-filter sequence.[19] The spectra were recorded at $\nu_0 = 104.26$ MHz on the Bruker ASX400 spectrometer. The spinning frequency was 15 kHz. The three pulses were experimentally optimised: the first hard pulse to 2.1 μs, the second hard pulse to 0.75 μs and the third selective *ca.* π/2 pulse to 6 μs.

Results and discussion

Characterization of the samples in the dried state

The prepared solids (Fig. 1) have P/Al atomic ratios varying from 0.03 to 0.2. The first value (equivalent to *ca.* 1.5 wt% P in the P-Al mixed oxide) is in the range of phosphorus contents where some hydrotreating reactions are effectively promoted by phosphorus addition in the catalyst.[5] The highest P/Al value (equivalent to *ca.* 8 wt% P) corresponds in general to less efficient catalysts; the reasons for this reduced efficiency have already been discussed.[3,5] In the dried state, only the two P/Al extremum compositions were considered in detail: those with

P/Al ratios of 0.03 and 0.2. For the first series of samples, the XRD patterns show broad peaks which are similar for each sample, P1, P2 or P3; they are characteristic of the presence of poorly crystallised boehmite. For the second series of samples, the XRD patterns indicate a large amorphous character for sample P1, while the patterns of samples P2 and P3 are characteristic of the presence of badly crystallised boehmite.

The ^{27}Al and ^{31}P MAS NMR spectra of the series of dried samples are reported in Fig. 2 and 3 respectively. For P/Al = 0.03, there is no difference between samples P1, P2, and P3 with a single ^{27}Al signal around $\delta_2^G \approx 7$ (Fig. 2a) which corresponds to the presence of octahedral aluminium sites[20] in an oxygen environment. In contrast, there is a small but significant evolution of the broad ^{31}P spectrum (Fig. 3a) whose apparent maximum moves from −7 ppm (sample P1) to *ca.* −19 ppm (sample P3). These spectra result from the superposition of peaks resulting from monomeric phosphate (−8 ppm) and polymeric phosphate species (−20 ppm) according to the literature data.[21] Therefore, monomers are the major P-oxo species for the P1 sample while, conversely, polyphosphates dominate in sample P3. The characteristics of the P2 spectrum at about −15 ppm indicate an almost equal distribution of both entities. In the series of samples with P/Al = 0.2, the introduction of phosphorus clearly influences the ^{27}Al spectrum (Fig. 2b). A weak peak at $\delta_2^G \approx 39$ is observed for samples P1(0.2)D-Al and P2(0.2)D-Al. This signal can be attributed to the presence of $AlPO_4$.[21] In contrast, when orthophosphoric acid is dissolved in water (step 3 in Fig. 1), mainly octahedral Al species ($\delta_2^G \approx 7$) can be observed with a very broad signal around $\delta_2^G \approx 60$. It is clear that the method of H_3PO_4 introduction has a rather important effect on the gel formation. For samples P1 and P2, the hydrolysis step involves ASB dissolved in a mixture of 2-butanol, 1,3-butanediol and H_3PO_4. For sample P3, H_3PO_4 is introduced in the water used for hydrolysis. The main difference could be the extent of dissociation of H_3PO_4 in such solvents and its ability to exchange ligands with ASB. This is confirmed by ^{31}P liquid-phase NMR experiments which reveal that H_3PO_4 is not dissociated in 2-butanol and in 1,3-butanediol, whereas it is dissociated in water. The relative permittivity of water is high ($\varepsilon = 78.5$ at 25 °C), whereas the values are smaller for alcohols

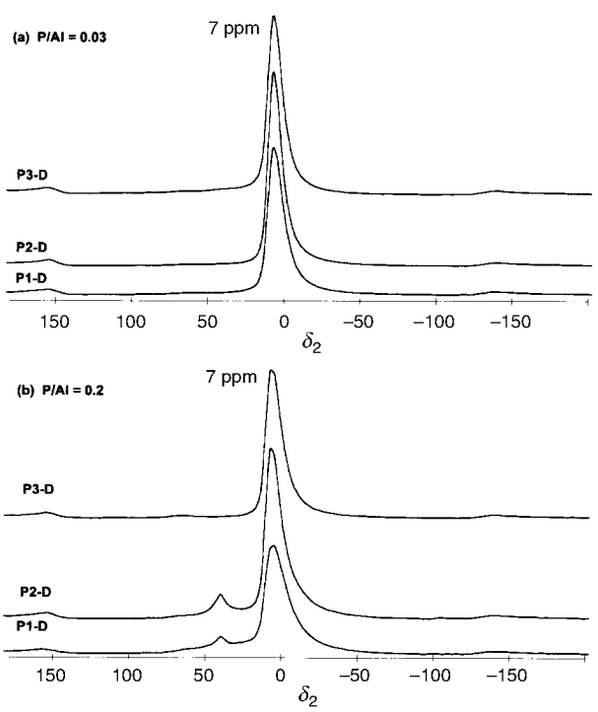

Fig. 2 ^{27}Al MAS NMR spectra of the dried solids: (a) samples with P/Al = 0.03, (b) samples with P/Al = 0.2.

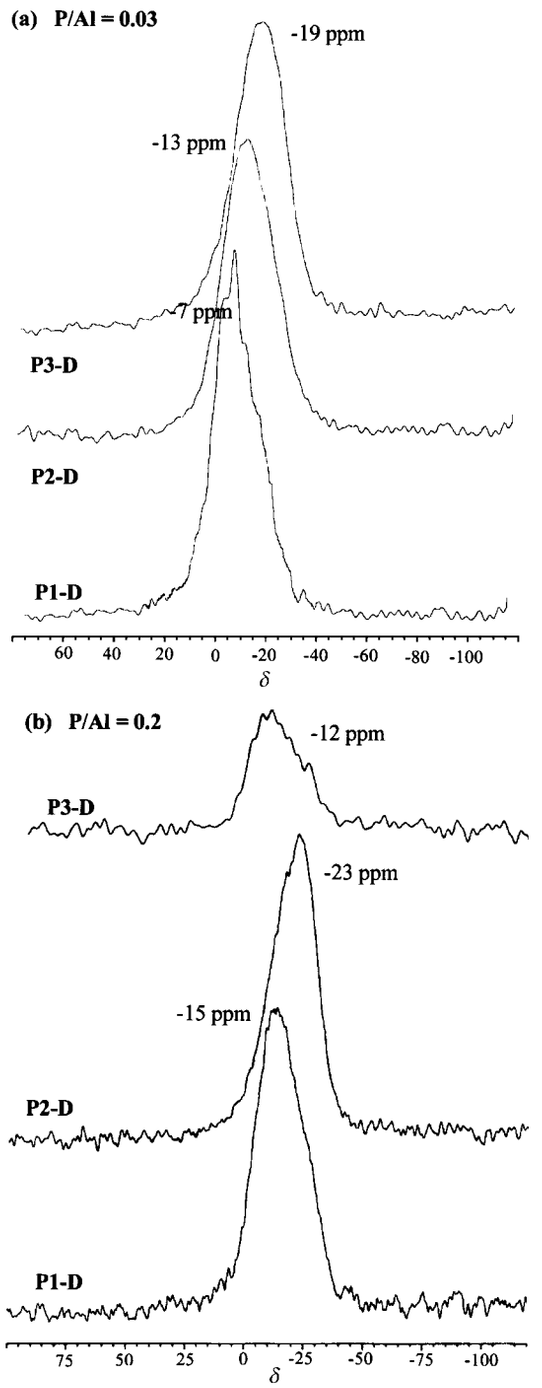

Fig. 3 ^{31}P MAS NMR spectra of the dried solids: (a) samples with P/Al = 0.03, (b) samples with P/Al = 0.2.

and decreasing with the number of carbons in the molecule (ε for 2-butanol is 15.8 at 25 °C). Even though the introduction of a second OH group into the molecule increases the ε value (*i.e.*, ε of 1-propanol is 20.1 and that of 1,2-propanediol is 32), it is clear that H_3PO_4 is weakly dissociated in steps 1 or 2, whereas it is partly dissociated in water ($pK_A = 2.1$, 7.2 and 12, respectively for H_3PO_4, $H_2PO_4^-$ and HPO_4^{2-}). Therefore, the butoxide ligands of ASB in the solvent can be (partially) exchanged, not only with 1,3-butanediol, but also with H_3PO_4 according to the following equilibrium:

$$Al(OR)_3 + xH_3PO_4 \rightleftharpoons (RO)_{3-x}Al[OPO(OH)_2]_x + xROH \quad (1)$$

After the hydrolysis–condensation steps, some of the phosphate ligands may remain bound to Al, contributing to the presence in the dried solids of Al_{tetra}–O–P sites which have a ^{27}Al NMR fingerprint at $\delta_2^G \approx 39$. Such species are not detected

by XRD due to the poor crystallinity of such compounds. They are not detected in the series corresponding to P/Al = 0.03 due to the equilibrium displacement towards $Al(OR)_3$. Moreover, the existence of a monomeric phosphate ligand for the P3(0.2)D-Al catalyst is confirmed by the ^{31}P NMR spectrum (Fig. 3b). Indeed, monomers (peak maximum ≈ -12 ppm) are the major P-oxo species for sample P3 while polyphosphates dominate in samples P2.

Characterization of the samples in the calcined state

As for the dried samples, only two compositions were firstly and extensively considered: P/Al = 0.03 and P/Al = 0.2. The carbon and phosphorus contents and the specific surface area (SSA) evolution are reported in Table 1 for both series. The amount of carbon is small and independent of the phosporus introduction method and amount of phosphorus. It can be concluded that most of the organic molecules (2-butanol and 1,3-butanediol) are removed during the successive drying and calcination procedures (Fig. 1). Concerning the SSA evolution (Table 1), an influence of the phosphorus introduction route is clearly visible. For both series P(0.03)C-Al and P(0.2)C-Al, the surface area decrease follows the trend: P1 $\approx$ P2 > P3. The difference between P1 and P2 is not very significant, whereas the loss in SSA is important for P3 catalysts. Moreover, the SSA values are lower for the solids corresponding to the ratio P/Al = 0.2 than for the other series.

For samples P1, P2 and P3 of low phosphorus content (P/Al = 0.03), the XRD patterns indicate the presence of very badly crystallised γ-alumina with mainly amorphous character. For the P(0.2)C-Al samples, the XRD patterns show structural differences depending on the method of preparation (Fig. 4). The results for P1 and P2 reveal the presence of rather amorphous γ-alumina while in sample P3, which was obtained with phosphoric acid dissolved in water, new peaks can be observed; the most intense are indicated with asterisks at $2\theta = 20.6$, 21.7, 26.4 and 35.8°. These new diffraction peaks could be attributed to different crystallised $AlPO_4$ phases, probably formed during the calcination step which transforms some monophosphate species adsorbed on the alumina gel during its formation in the hydrolysis step (Fig. 1).

The ^{27}Al and ^{31}P MAS NMR spectra are reported in Fig. 5 and 6, respectively. For the sample series with P/Al = 0.03, there is no clear difference in the ^{27}Al spectra between P1, P2 and P3 (Fig. 5a), with three peak maxima around $\delta_2^G \approx 6$, 30 and 64, corresponding respectively to octahedral, pentacoordinate and tetrahedral aluminium sites in an oxygen environment.[20,22] When comparing the ^{31}P spectra of the dried (Fig. 3a) and calcined (Fig. 6a) samples, the same peaks evolution from P1 to P3 is observed. For the dried samples, the peak maximum shifts from −7 to −19 ppm whereas, for the calcined samples, the peak maximum shifts from −11 to −23 ppm. This evolution indicates the presence of mainly monomeric phosphates in P1, whereas mixtures of monomeric and polyphosphates are present in P2 and P3.

For the calcined samples of the series with P/Al = 0.2, the introduction of phosphorus clearly has an influence on the ^{27}Al spectra (Fig. 5b). Octahedral ($\delta_2^G \approx 6$) and tetrahedral ($\delta_2^G \approx 60$) aluminium sites are observed, and also a peak at $\delta_2^G \approx 39$ corresponding to $AlPO_4$. The concentration of $AlPO_4$ increases when the introduction of H_3PO_4 is delayed. Moreover, for sample P3 a shoulder can be observed around $\delta_2^G \approx 30$, but it is difficult to confirm the presence of this peak for the other samples, P1 and P2. There is also evolution of the broad ^{31}P spectra (Fig. 6b): the apparent maximum is around −21 ppm for P1 and −24 ppm for P2 and characterizes the presence of polymeric phosphate species. For the P3(0.2)C-Al catalyst, a sharper peak at −27 ppm, which may be characteristic of crystalline $AlPO_4$,[22] is also observed.

3QMAS NMR was performed to better identify the different aluminium sites with their actual isotropic chemical shifts and their quadrupolar interactions in the P(0.03)C-Al and P(0.2)C-Al sample series. Indeed, when the nucleus spin number is greater than ½, the nucleus possesses an electric quadrupole momentum that interacts with the electric field gradients at the nucleus. The resulting quadrupolar effects are strongly linked to the local surrounding symmetry of the nucleus. Apart the line broadening resulting from the quadrupolar interaction, another important effect can be noted: the resonances are shifted from the true isotropic chemical shifts (δ_{CS}) by the quadrupole-induced shifts (δ_{QIS}) which are only dependent on

Table 1 Chemical composition and specific surface area (SSA) of the calcined (500 °C) P-alumina solids

Catalyst	wt% C	wt% P	P/Al	SSA/$m^2\ g^{-1}$
P1(0.03)C-Al	0.06	1.73	0.033	567
P2(0.03)C-Al	0.38	2.07	0.028	610
P3(0.03)C-Al	0.11	1.44	0.026	493
P1(0.07)C-Al	0.29	3.79	0.07	515
P1(0.2)C-Al	0.83	7.87	0.21	524
P2(0.2)C-Al	1.25	8.37	0.18	515
P3(0.2)C-Al	0.44	7.77	0.19	335

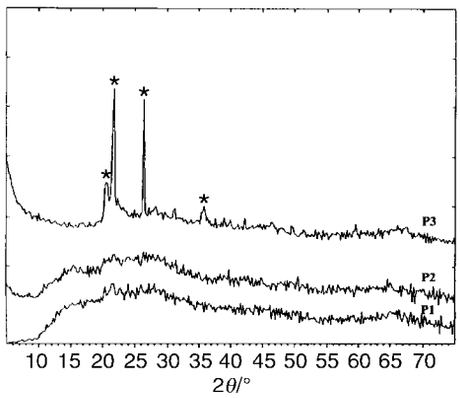

Fig. 4 XRD patterns of samples P1, P2 and P3 of the P(0.2)C-Al series.

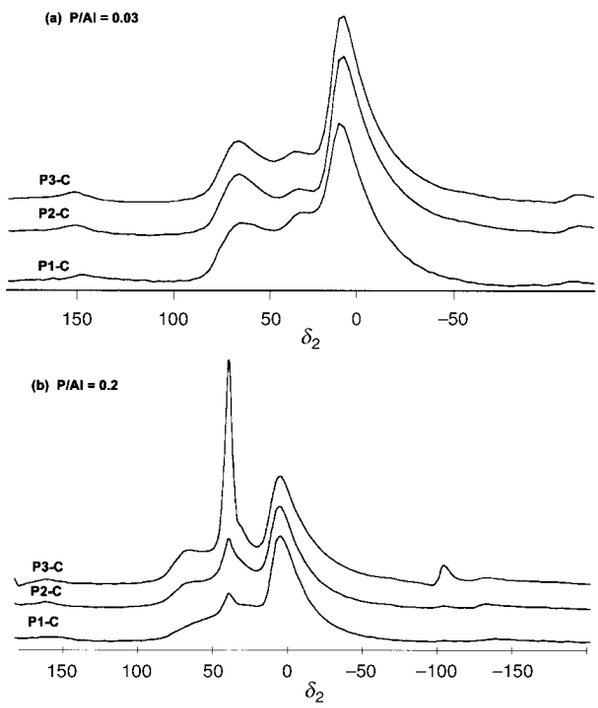

Fig. 5 ^{27}Al MAS NMR spectra of the calcined (500 °C) solids: (a) samples with P/Al = 0.03, (b) samples with P/Al = 0.2.

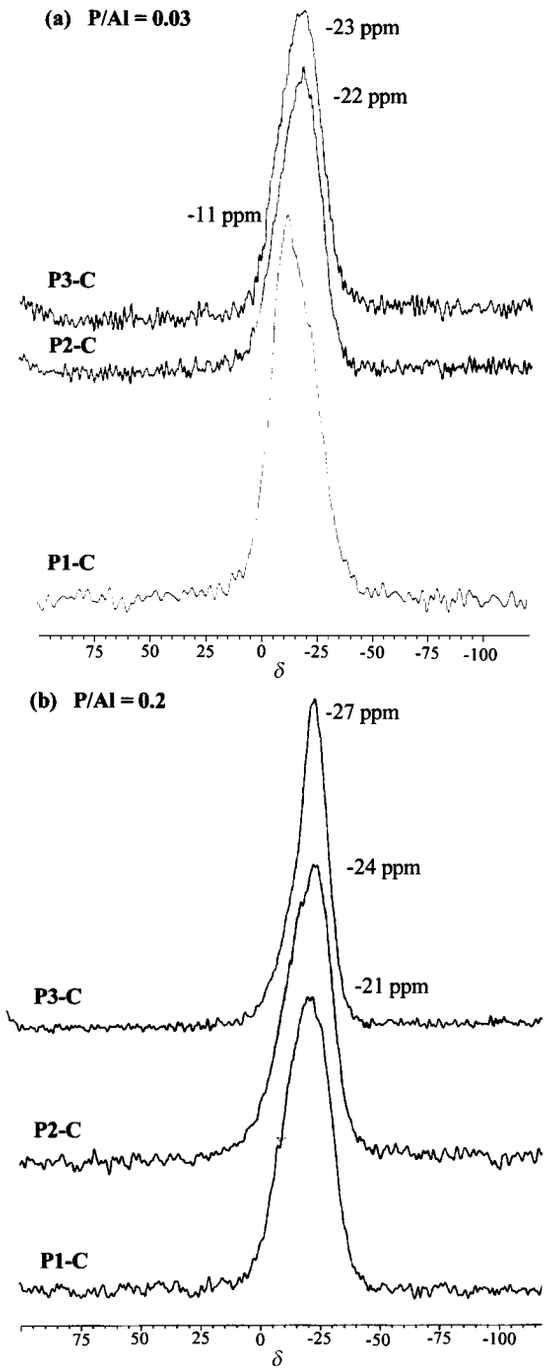

Fig. 6 ^{31}P MAS NMR spectra of the calcined (500 °C) solids: (a) samples with P/Al = 0.03, (b) samples with P/Al = 0.2.

the amplitude of the quadrupole interactions. It follows that corrections must be performed to obtain the actual chemical shifts whose values must be considered when comparing the various samples. This is possible using MQMAS spectra.

After shearing the 2D 3QMAS spectrum, we can define in ppm the two principal axes: δ_2 and δ_{iso}. The projection of the 2D spectrum onto the δ_2 axis leads to the 1D MAS spectrum filtered in 3 Quanta. An orthogonal projection of the 2D spectrum on the δ_{iso} axis leads to the high resolution 1D spectrum.

On the 2D spectrum (Fig. 7), we can draw two particular lines: the chemical shift (CS) axis, which gives the location of the resonance (true isotropic chemical shift) in the absence of quadrupolar interaction, and the quadrupolar induced shift (QIS) direction.[19] On the one hand, projections of the center of gravity of each resonance on the CS axis along the QIS

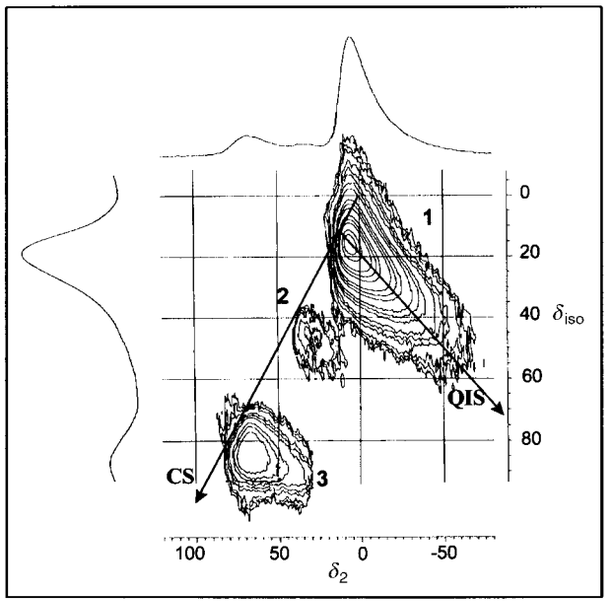

Fig. 7 ^{27}Al 3QMAS NMR sheared spectrum of the calcined (500 °C) P1(0.03)C-Al sample.

direction (slope = −10/17) permit the determination of the actual isotropic chemical shifts (δ_{CS}). On the other hand, the distance of the center of gravity from the CS axis along the QIS direction allows one to determine the second order quadrupolar effect, SOQE = $C_Q(1+\eta_Q^2/3)^{\frac{1}{2}}$.[19] For each species, the actual chemical shift can also be deduced from the position of the centers of gravity (δ_2^G) of its resonance by the relation (for $S = 5/2$):

$$\delta_{CS} = \delta_2^G + \delta_{QIS} = \delta_2^G - 6000(SOQE/\nu_0)^2 \qquad (2)$$

In addition, if the surrounding of a nucleus is perfectly determined, the corresponding sheared resonance is very narrow and parallel to the δ_2 axis (Fig. 7). Conversely, any vertical spreading of the sheared resonances may indicate a distribution of chemical shift and/or quadrupolar interaction.

Fig. 7 reports the typical ^{27}Al 3QMAS NMR spectra of the P1(0.03)C-Al sample. The corresponding P2 and P3 two-dimensional (2D) spectra are quite similar. Octahedral ($\delta_2^G = 6$), pentacoordinate ($\delta_2^G = 29$) and tetrahedral ($\delta_2^G = 64$) aluminium sites are clearly identified. The corresponding isotropic chemical shifts and the second order quadrupolar effect (SOQE) values, are reported in Table 2. We also observed a significant distribution of the octahedral site resonances preferentially along the QIS direction, which denotes a spreading of the SOQE parameter. The averaged SOQE values for each species of the P(0.03)C-Al sample series (Table 2) are however similar, whatever the method of preparation ($\approx$3.2 MHz for species 1, $\approx$4.3 MHz for species 2 and 3). This means that, at low P content, the structure of the alumina lattice is apparently not significantly perturbed by the phosphorus addition.

For the P(0.2)C-Al sample series, the ^{27}Al 3QMAS NMR results are very different for the three preparation methods, as shown in Fig. 8. Three different species are easily detected for samples P1(0.2)C-Al (Fig. 8a) and P2(0.2)C-Al (Fig. 8b), whereas at least four species are observable in sample P3(0.2)C-Al (Fig. 8c). For the three catalysts, zones corresponding to species s1 (octahedral aluminium) and s3 (tetrahedral aluminium) are oriented along the QIS direction, which indicates a distribution of electric field gradients and therefore that the corresponding sites are incorporated in an amorphous structure. Sample P3 exhibits substantial modifications of the remaining central zone. Indeed, a detailed analysis of this resonance shows the previous s2 species (pentacoordi-

Table 2 Averaged δ_2^G(resonance frequency), δ_{CS} (chemical shift) and SOQE values obtained by ^{27}Al 3QMAS NMR of the P(0.03)C-Al sample series

	P1(0.03)C-Al			P2(0.03)C-Al			P3(0.03)C-Al		
	δ_2^G	δ_{CS}	SOQE/MHz	δ_2^G	δ_{CS}	SOQE/MHz	δ_2^G	δ_{CS}	SOQE/MHz
Species 1	6.4	12	3.2	6.5	12	3.2	6.3	12	3.2
Species 2	29	39	4.3	29.3	39	4.2	29	39	4.2
Species 3	64.4	75	4.4	64.5	75	4.4	64.4	75	4.4

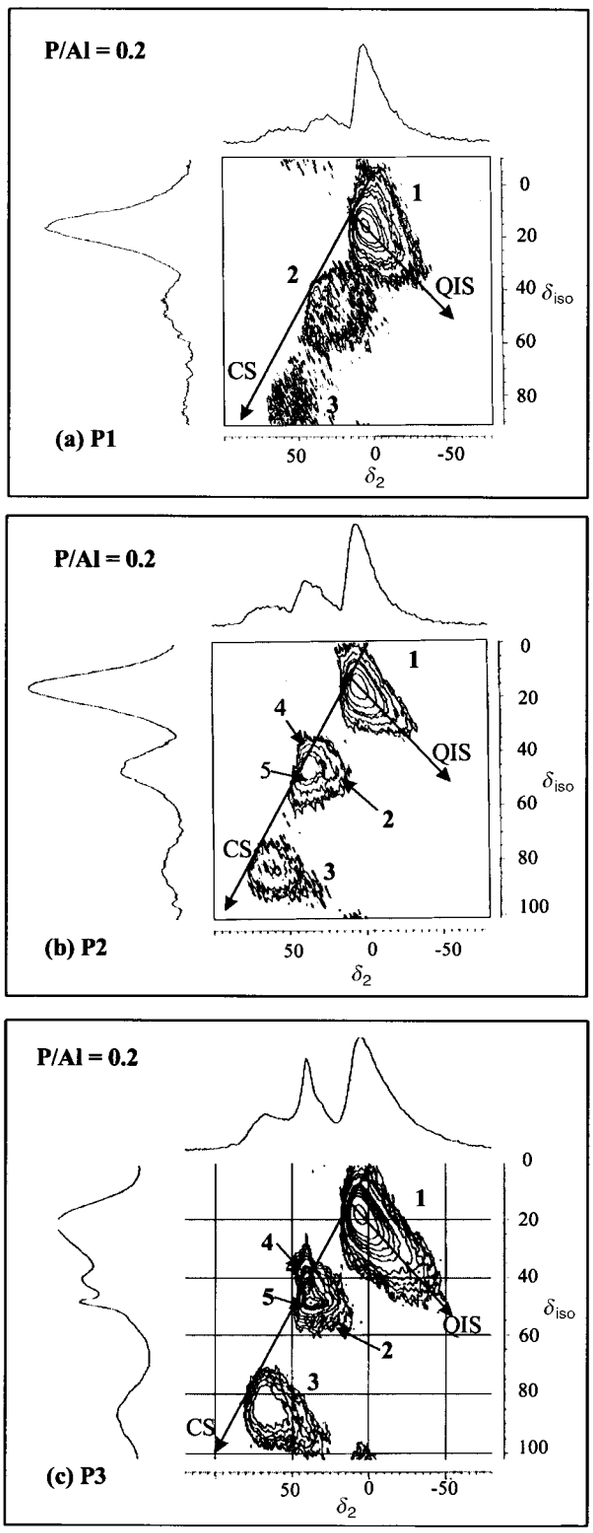

Fig. 8 ^{27}Al 3QMAS NMR sheared spectra of the calcined (500 °C) solids of the series P(0.2)C-Al. (a) sample P1(0.2)C-Al, (b) sample P2(0.2)C-Al, (c) sample P3(0.2)C-Al.

nate aluminium) and also two other species: s4 ($\delta_2^G = 40$) and s5 ($\delta_2^G = 34$). The fourth species corresponds to the aluminium phosphate identified in 1D spectra ($\delta_2^G = 39$). The fifth species, not identified on the 1D spectra, is attributed to another aluminium phosphate species. The narrow line of this new species indicates that this site is present in sample P3(0.2)C-Al, with a structure of good crystallinity.

In fact, in P2 and P3 catalysts there is also some s4 aluminium phosphate ($\delta_2^G = 39$). This species is observed in the 1D spectra (Fig. 5) but not in the 3QMAS spectra (Fig. 8a and b). This is due to two reasons: (i) its concentration in samples P1 and P2 is lower than in catalyst P3, and (ii) the efficiency of the MQMAS experiment does not permit the observation of species with low SOQE values. Indeed the SOQE of species 4 is 1.8 MHz (Table 3) and is much smaller than all the other species.

In the spectrum of P1 (Fig. 8a) we essentially observe in the central zone the s2 species ($\delta_2^G = 29$) and a small amount of s4 ($\delta_2^G = 39$). In the case of the P2 sample (Fig. 8b), we note an evolution of the central resonance which shows the formation of a small amount of species s5. As for the previous series of samples, the SOQE of each species can be calculated from the center of gravity of the corresponding zone (Table 3), but the spreading of the resonances along the QIS direction leads to some uncertainty to the reported values. Therefore, only the main trends in the data evolution when comparing the preparation procedures P1, P2 and P3 will be considered. The quadrupolar effect (around 3.2 MHz) of the octahedral aluminium sites (species 1, $\delta_{CS} = 11$) has not changed. In contrast, tetrahedral aluminium sites (species 3, $\delta_{CS} = 75$) have a significant decrease (5.2 MHz to 4.3 MHz) of the quadrupolar effect. The SOQE value of pentacoordinate aluminium, species 2 ($\delta_{CS} \approx 39$–41) cannot be clearly evaluated, as there is an overlap between the NMR resonance of this species and those of species 4 and 5.

Clearly, introduction of phosphorus with P/Al = 0.2 has a strong influence on the pentacoordinate aluminium sites. As an example, P3 preparation introduces a large amount of another aluminium site (species 5, $\delta_{CS} = 45$) which corresponds to well crystallised aluminium phosphate already detected by XRD (Fig. 4). Its origin could be due, as discussed before, to transformation of phosphates deposited on the alumina during its formation by hydrolysis. Therefore, some of the phosphorus in the P3 sample preparation should be located within the alumina framework (leading to more symmetric pentacoordinate aluminium), and some may exist as $AlPO_4$ deposited on the P-doped alumina. It is important to note that 3QMAS experiments clearly show the formation of two new species in the case of the P3 preparation, whereas 1D MAS spectra and XRD patterns only show one species.

In short, the phosphorus introduction step in the sol–gel preparation has very important consequences for the structure of the P-doped alumina after calcination. For P1–Al samples, phosphorus is mainly present as monomeric phosphate, well dispersed on the alumina surface and with very weak interactions with the aluminium sites. In P2 samples, the amount of polymeric phosphate increases with the formation of amorphous aluminium phosphate. The pentacoordinate aluminium sites begin to be involved in the interaction. In P3 samples, the dissociation of phosphoric acid in water leads to

Table 3 Averaged δ_2^G (resonance frequency), δ_{CS} (chemical shift) and SOQE values obtained by ^{27}Al 3QMAS NMR of the P(0.2)C-Al sample series

	P1(0.2)C-Al			P2(0.2)C-Al			P3(0.2)C-Al		
	δ_2^G	δ_{CS}	SOQE/MHz	δ_2^G	δ_{CS}	SOQE/MHz	δ_2^G	δ_{CS}	SOQE/MHz
Species 1	5.6	11	3.2	5.9	11	3.0	6.4	12	3.2
Species 2	29	39	4.2	[a]	[a]	[a]	[a]	[a]	[a]
Species 3	61	75	5.2	64	75	4.5	64	75	4.3
Species 4	39	[a]	[a]	39	[a]	[a]	40	42	1.8
Species 5	[a]	[a]	[a]	[a]	[a]	[a]	34	45	4.4

[a]Undetermined: low intensity, overlapping resonances.

the formation of a well defined crystallised aluminium phosphate phase on alumina, which also contains phosphates in its structure.

Influence of the phosphorus content

For the study of the effect of the phosphorus content on the morphology of the P-alumina samples, procedure P1 was chosen, as it was shown previously that this procedure leads to better dispersed phosphate species. As spectra of the P1(0.03)-Al and P1(0.2)-Al samples have already been analysed, comparisons will be based on the sample with the intermediate P/Al = 0.07 composition. For the dried samples, the XRD patterns do not indicate the presence of crystallised phases, whatever the phosphorus content, and it seems that the amorphous character increases with increasing phosphorus content.

Fig. 9 and 10 permit the comparison of the ^{27}Al and ^{31}P MAS NMR spectra of the samples prepared with procedure P1 and with different P/Al ratios. For the dried samples, the feature at $\delta_2^G = 39$ characteristic of the presence of aluminium phosphates is already detected for P/Al = 0.07, whereas it is not for P/Al = 0.03 (Fig. 9a). Moreover, from ^{31}P NMR (Fig. 10a), it appears that the proportion of polymeric phosphate increases with the P content as evidenced by the increase of the component at ≈ -20 ppm.

The compositions of the calcined samples are compared in Table 1. There is a gradual increase of the remaining carbon content with the amount of phosphorus introduced in the samples, but this always remains low (from 0.06 to 0.83 wt%). Conversely, the specific surface area remains larger than 500 $m^2\ g^{-1}$, whatever the phosphorus content, for P1 samples. The ^{27}Al NMR features of the calcined samples are compared in Fig. 9b. For the P1(0.07)C-Al and P1(0.2)C-Al samples, main peaks are observed at $\delta_2^G = 6$, 39 and 64 corresponding respectively to octahedral aluminium, Al–O–P oxo species and tetrahedral aluminium. For the P1(0.03)C-Al sample, the peak at $\delta_2^G = 39$ is not observed, but the pentacoordinate aluminium species at $\delta_2^G = 29$ is clearly identified. The increasing amount of phosphorus is also responsible for the evolution of the phosphorus spectra (Fig. 10b). The main species are monomeric phosphate for P(0.03)C-Al, a mixture of monomeric and polymeric phosphates for P(0.07)C-Al and essentially polymeric phosphates and $AlPO_4$ for sample P(0.2)C-Al. The 3QMAS spectrum of sample P1(0.07)C-Al is similar to those already presented (Fig. 7 and 8a) and the characteristic data are reported in Table 4. The chemical shifts are similar for each species whatever the amount of phosphorus. From the SOQE values, it appears that the electronic environment of the octahedral and pentacoordinate aluminium species is not influenced by the increasing amount of introduced phosphorus whereas that of tetrahedral aluminium is (SOQE = 4.4 MHz, 4.7 MHz and 5.2 MHz respectively for P1(0.03), P1(0.07) and P1(0.2)). This may be due to the fact that some Al–O–P groups are in the local environment of the tetrahedral aluminium sites, which increases their distortion.

Influence of the temperatures of drying and calcination

In the sol–gel procedure for the preparation of pure or mixed oxides from alkoxides, the drying step allows the elimination of any excess water, used for hydrolysis, and the alcohol(s), whereas calcination leads to the formation of the final architecture of the oxide(s). In the previous sections, samples were dried at 100 °C and then calcined at 500 °C. Here, the influences of drying temperature (room temperature RT, 100 °C or 200 °C during one night) and of calcination (from 350 to 700 °C for 3 h) will be examined for samples obtained by the P1 procedure. Table 5 shows that the temperature of calcination has a non-negligible influence on the specific surface area of the P1 samples, whereas drying or the phosphorus content have no appreciable effect.

For samples P1(0.03)-Al, ^{27}Al NMR spectra of the dried gels are similar to that reported in Fig. 2(a) for drying temperatures up to 200 °C with a main peak at $\delta_2^G = 6$ characteristic of octahedral aluminium species. Clearly, treatment at 200 °C has no influence on the gel transformation. However, it appears that the subsequent calcination transforms the initial gel as shown by the NMR spectra in Fig. 11. Indeed, after calcination at 350 °C (Fig. 11b), in addition to the octahedral aluminium ($\delta_2^G = 6$) peak, the appearance of broad features in the high chemical shift range is observed. This evolution is probably due to the transformation of pseudoboehmite into γ-alumina. Upon calcination at higher temperatures (Fig. 11c to 11g),

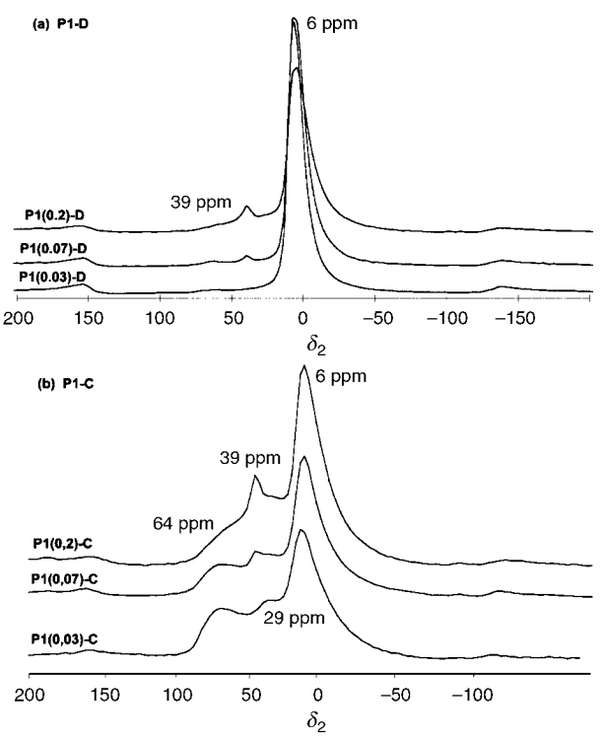

Fig. 9 ^{27}Al MAS NMR spectra of the P1 samples with different P/Al ratios: (a) dried samples, (b) calcined samples.

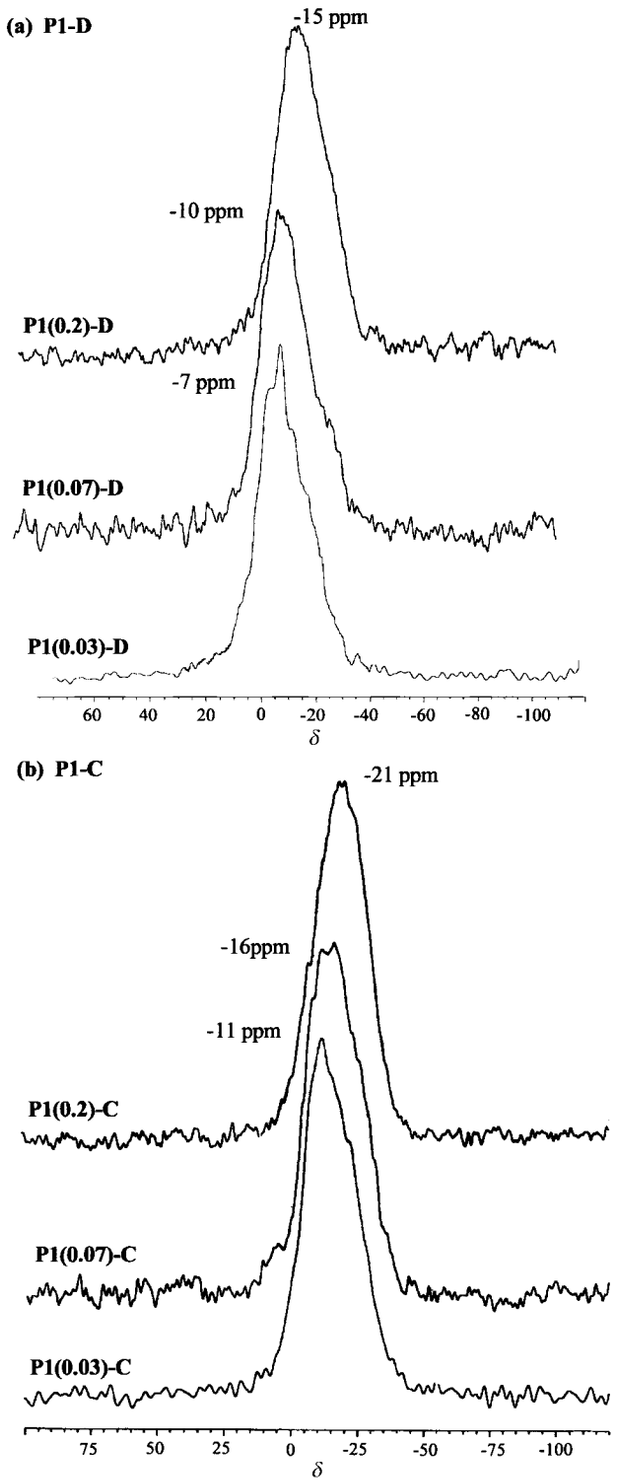

Fig. 10 ^{31}P MAS NMR spectra of the P1 samples with different P/Al ratios: (a) dried samples, (b) calcined samples.

these features are more developed with peaks at $\delta_2^G = 29$ (pentacoordinate aluminium) and $\delta_2^G = 64$ (tetrahedral aluminium). Qualitatively, calcination temperatures in the 500–700 °C range do not influence the relative proportions of these species. In addition, as XRD does not detect any changes, it seems that the rather amorphous alumina which is formed under these calcination conditions is stable. Fig. 12 presents the evolution of the ^{31}P NMR spectra upon calcination. The increase of the calcination temperature induces an increase of the proportion of monomeric phosphates and conversely a decrease of the polymeric phosphate species. This result is in agreement with the observations of DeCanio *et al.*[21] who

Table 4 Averaged δ_2^G (resonance frequency), δ_{CS} (chemical shift) and SOQE values obtained by ^{27}Al 3QMAS NMR of the P(0.07)C-Al sample

	δ_2^G	δ_{CS}	SOQE/MHz
Species 1	5.6	11	3.2
Species 2	28	39	4.5
Species 3	64	76	4.7
Species 4	40	[a]	[a]

[a]Undetermined: low intensity, overlapping resonances.

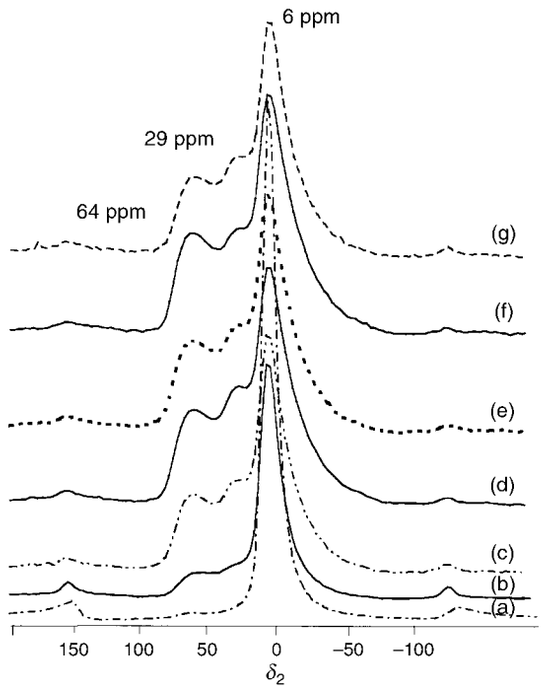

Fig. 11 ^{27}Al NMR spectra of P1(0.03)-Al samples after different conditions of drying (D) and calcination (C): (a) D = 100 °C; (b) D = 100 °C, C = 350 °C; (c) D = RT, C = 500 °C; (d) D = 100 °C, C = 500 °C; (e) D = 200 °C, C = 500 °C; (f) D = 100 °C, C = 600 °C; (g) D = 100 °C, C = 700 °C.

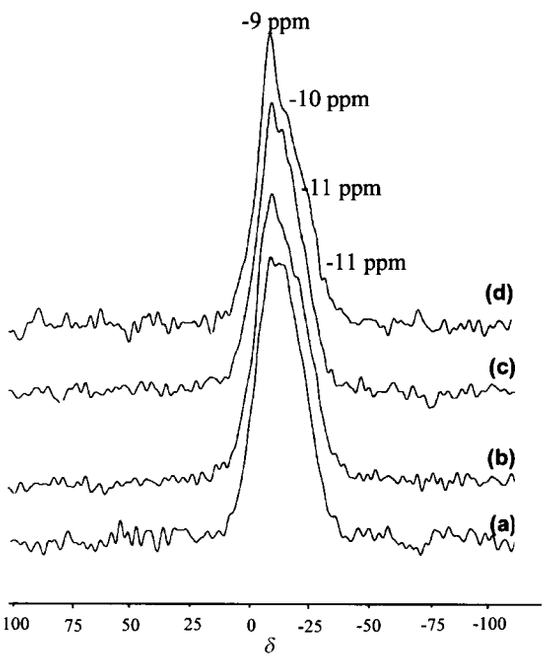

Fig. 12 ^{31}P NMR spectra of the P1(0.03)-Al sample dried at 100 °C and calcined at different temperatures: (a) 350 °C, (b) 500 °C, (c) 600 °C and (d) 700 °C.

Table 5 Specific surface area ($m^2\ g^{-1}$) of the P-Al samples after different drying (overnight) and calcination temperatures (3 h)

Temperature of drying/°C	Temperature of calcination/°C	P1(0.03)-Al	P1(0.07)-Al	P1(0.2)-Al
RT	350	673	—	—
RT	500	587	—	—
RT	700	381	—	—
100	350	669	573	665
100	500	567	515	524
100	600	448	—	—
100	700	363	458	388
200	350	604	—	—
200	500	590	—	—
200	700	426	—	—

showed that calcination at 500 °C leads to a decrease of the amount of polymeric phosphate and simultaneously to the formation of well dispersed amorphous aluminium phosphates.

For the P1 samples with P/Al = 0.07 and P/Al = 0.2, the ^{27}Al NMR spectra (Fig. 13 and 14) show that the major evolution occurs at 350 °C or higher. At high temperatures, from 350 to 700 °C, a small amount of $AlPO_4$ species ($\delta_2^G = 39$) and tetrahedral aluminium species are observed. Their proportions, relative to octahedral aluminium, increase with the temperature of calcination. Indeed, for sample P1(0.2)C-Al calcined at 700 °C, the signal at $\delta_2^G = 39$ is dominant. We can conclude that in the case of large amounts of P (P/Al = 0.2), there is (partial) destruction of the structure of alumina with formation of $AlPO_4$ when the calcination temperature increases.

Conclusion

The sol–gel procedure used in this work for the formation of P-alumina catalytic supports leads to different results concerning the local structure of the Al and P atoms depending on the step where orthophosphoric acid is introduced. It appears that when H_3PO_4 is introduced with 2-butanol (samples P1), the phosphorus-oxo species are better dispersed in/on the aluminium oxide framework, mainly as monomeric phosphate groups. The oxide matrix, in the form of poorly crystallised pseudo-boehmite after gel drying, is transformed into rather amorphous γ-alumina after calcination at 350 °C or higher. In contrast, dissolution of H_3PO_4 in water (samples P3) leads to a quite different system, with evidence for the presence of Al_{tetra}–O–P bridges in the dried gels. Upon calcination, these species contribute to the formation of crystallised $AlPO_4$. Moreover, NMR characterisation has shown that the phosphorus loading influences the relative proportion of each species. For higher calcination temperatures and the highest P/Al ratio (P/Al = 0.2), there is destruction of alumina with formation of aluminium phosphate. High calcination temperatures also have a detrimental effect on the specific surface area of the samples which, however, remains as high as 350 $m^2\ g^{-1}$.

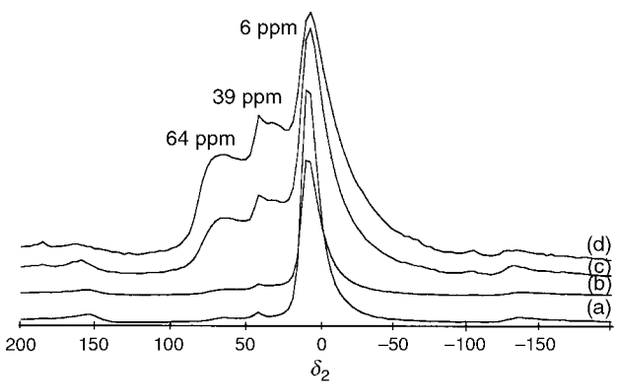

Fig. 13 ^{27}Al NMR spectra of ample P1(0.07)-Al dried at 100 °C (a) and calcined at different temperatures: (b) 350 °C, (c) 500 °C, (d) 700 °C.

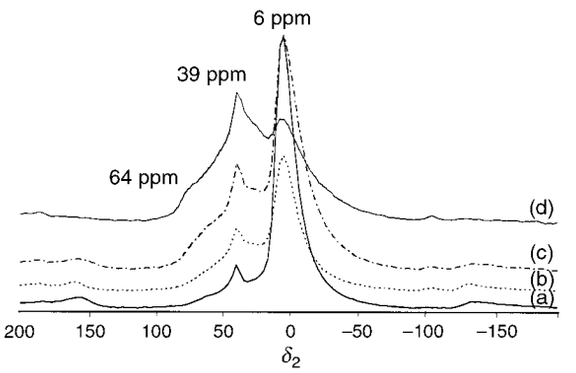

Fig. 14 ^{27}Al NMR spectra of sample P1(0.2)-Al dried at 100 °C (a) and calcined at different temperatures: (b) 350 °C, (c) 500 °C, (d) 700 °C.

Acknowledgements

The authors thank B. Revel from the Centre Commun de Mesures RMN de l'Université des Sciences et Technologies de Lille for its help and technical support. The Région Nord Pas de Calais is also acknowledged for financial support for the purchase of the ASX400 and ASX100 spectrometers. Bruker company is also acknowledged for scientific collaboration.

References

1 J. Grimblot, *Catal. Today*, 1998, **41**, 111.
2 H. Topsøe, B. S. Clausen and F. E. Massoth, *Hydrotreating Catalysis*, Springer-Verlag, Berlin, Heidelberg, 1996, and references therein.
3 R. Iwamoto and J. Grimblot, *Stud. Surf. Sci. Catal.*, 1997, **106**, 195.
4 R. Iwamoto and J. Grimblot, *J. Catal.*, 1997, **172**, 252.
5 R. Iwamoto and J. Grimblot, *Adv. Catal.*, 1999, **44**, 417.
6 M. Jian and R. Prins, *Catal. Lett.*, 1995, **35**, 193.
7 S. Eijbouts, L. Van Gruijthuijsen, J. Volmer, V. H. J. de Beer and R. Prins, *Stud. Surf. Sci. Catal.*, 1989, **50**, 79.
8 S. Eijsbouts, J. N. M. Van Gestel, J. A. R. Van Veen, V. H. J. de Beer and R. Prins, *J. Catal.*, 1991, **131**, 412.
9 H. Topsøe, B. S. Clausen, N. Y. Topsøe and P. Zeuthen, *Stud. Surf. Sci. Catal.*, 1989, **53**, 77.
10 E. Etienne, E. Ponthieu, E. Payen and J. Grimblot, *J. Non-Cryst. Solids*, 1992, **147–148**, 764.
11 L. Le Bihan, C. Mauchaussé, L. Duhamel, J. Grimblot and E. Payen, *J. Sol–Gel Sci. Technol.*, 1994, **2**, 837.
12 H. Krauss, R. Prins and A. P. M. Kentgens, *J. Phys. Chem.*, 1996, **100**, 16336.
13 R. Iwamoto, C. Fernandez, J. P. Amoureux and J. Grimblot, *J. Phys. Chem. B*, 1998, **102**, 4342.
14 L. Le Bihan, E. Payen and J. Grimblot, to be published.
15 J. P. Amoureux, C. Fernandez and S. Steuernagel, *J. Magn. Reson. A*, 1996, **123**, 116.

16 C. Fernandez, J. P. Amoureux, J. M. Chezeau, L. Delmotte and H. Kesseler, *Microporous Mater.*, 1996, **6**, 331.
17 A. Medek, J. S. Hardwood and L. Frydman, *J. Am. Chem. Soc.*, 1995, **117**, 12779.
18 D. Massiot, B. Touzo, D. Trumeau, J. P. Coutures, J. Virlet, P. Florian and P. J. Grandinetti, *Solid State Nucl. Magn. Reson.*, 1996, **6**, 73.
19 J. P. Amoureux and C. Fernandez, *Solid State Nucl. Magn. Reson.*, 1998, **10**, 211.
20 Y. Kurokawa, Y. Kobayashi and S. Nakaka, *Heterogeneous Chem. Rev.*, 1994, **1**, 309.
21 E. C. DeCanio, J. C. Edwards, T. R. Scalzo, D. A. Storm and J. W. Bruno, *J. Catal.*, 1991, **132**, 498.
22 S. H. Risbud, R. J. Kirkpatrick, A. P. Tagliavore and B. Montez, *J. Am. Ceram. Soc.*, 1987, **70**, C10.

Paper 9/03889B